

## Antiplasticization and Abrasion Resistance of Polycarbonates in the Charge-Transport Layer of an Organic Photoconductor

R. E. Cais,\* M. Nozomi, M. Kawai, and A. Miyake

Research Center, Imaging Materials Laboratory, Mitsubishi Kasei Corporation, 1000, Kamoshida-cho, Midori-ku, Yokohama 227, Japan

Received March 11, 1992; Revised Manuscript Received May 1, 1992

**ABSTRACT:** A correlation has been found between the abrasion resistance of polycarbonate layers of an organic photoconductor and the dynamic mechanical loss modulus of the glassy phase. In particular, the effect of diphenylhydrazone charge-transport molecules on the properties of various polycarbonate binder resins was studied by tensile testing and dynamic mechanical analysis. Dilution of polycarbonate by diphenylhydrazones lowers the  $T_g$  and simultaneously increases the tensile strength and modulus, with a transition from ductile to brittle failure. This antiplasticization is accompanied by a suppression of the intensity and distribution of sub- $T_g$  mechanical relaxations in the polycarbonate matrix. The degree of antiplasticization correlates with molecular mobility and free volume in the amorphous state. The abrasion rate of the charge-transport layer of an organic photoconductor, formulated from the above components, was measured by the Taber test. Resistance to abrasion involving cyclic fatigue depends on the structure and composition of the polycarbonate-diluent system and correlates with the strength and position of the sub- $T_g$  dynamic mechanical relaxation.

### Introduction

At present, the most suitable photoreceptor for low- and medium-speed electrophotographic plain-paper copiers and laser printers is a double-layered organic photoconductor. Photogeneration of carriers (electron-hole pairs) takes place in a thin charge generation layer (typically 0.5  $\mu\text{m}$ ), which is coated on a conductive substrate such as an aluminum drum. After photogeneration, mobile carriers (usually holes) are injected into a thicker charge-transport layer (about 25  $\mu\text{m}$ ), under an electric field gradient provided by a negative surface charge. These holes drift to the outermost layer of the photoreceptor to selectively neutralize surface charge, thereby forming a latent electrostatic image, which is subsequently developed by a thermoplastic toner.<sup>1</sup>

The charge-transport layer is formulated from two major components. They are electron-donor molecules responsible for hole transport and an appropriate binder resin. It must be amorphous and transparent to light. Charge-transport molecules are usually low molecular weight organic compounds with arylamine or hydrazone groups, and they are selected primarily on the basis of their solubility, compatibility with the binder resin, charge-transport property, and electrophotographic cyclic stability. The charge-transport molecule is a nonreactive binder resin diluent (molecular dopant), and it must be compatible in approximately equal parts by weight to ensure good charge mobility, which involves electron hopping between adjacent charge-transport molecules.

The role of the binder resin is to impart physical durability. Perhaps the most suitable binder resins are the aromatic polycarbonates (PCR), which exhibit such desirable characteristics as solubility (to allow film coating from solution), high carrier mobility, compatibility with charge-transport molecules, transparency, durability, adhesion to the charge generation layer, and so on. The simplest and best known is Bisphenol A polycarbonate (BPA-PCR), which has excellent impact strength and toughness. However, these attributes of pure polymer are modified by dilution with low molecular weight additives

like charge-transport molecules. Some additives may act as a plasticizer,<sup>2</sup> increasing ductility and flexibility, whereas others may show the opposite effect of an antiplasticizer,<sup>3</sup> increasing brittleness and modulus. The role of additives depends on their size, shape, polarity, and concentration,<sup>4</sup> but the detailed mechanism of antiplasticization is still a topic for continuing research.<sup>5,6</sup>

Therefore, the mechanical behavior of the charge-transport layer is a *system* property, characteristic of a particular binder resin-charge-transport molecule combination. Mechanical properties determine the service lifetime of an organic photoconductor, which is reduced by scratching and abrasion during the copy (print) process, owing to physical contact of the surface of the charge-transport layer with paper and machine components designed for the addition and removal of toner. To date, there have been few studies published concerning the bulk properties of molecularly-doped polycarbonates in organic photoconductors.<sup>7,8</sup> These limited reports about fundamental properties are in contrast to the vast applied patent literature on the abrasion resistance of photoreceptors for commercial copy machines.

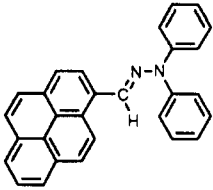
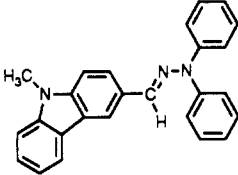
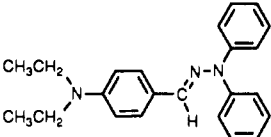
Industrial production of organic photoconductors is by dip coating from solution, but in this work melt compounding and injection molding was used to fabricate thick samples suitable for mechanical testing. The aim of the present study of the mechanical behavior of glassy solutions of diphenylhydrazones in polycarbonates is to gain some better understanding of the relationship between the molecular structure and material properties of organic photoconductors, particularly their abrasion resistance. It is anticipated that such insight will provide a systematic guideline for designing new photoconductors with an improved lifetime.

### Experimental Section

**Materials.** Three diphenylhydrazone (DPH) derivatives were utilized. They are denoted PY-DPH, CZ-DPH, and EA-DPH, according to the structure of their precursor aldehyde. These charge-transport molecules were electrophotographic-grade materials with at least 98% purity and were synthesized by the usual procedure. They were selected to offer a range of densities, glass transition temperatures ( $T_g$ ), and conformational flexibility, which may systematically influence their effect on mechanical

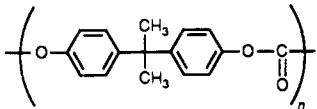
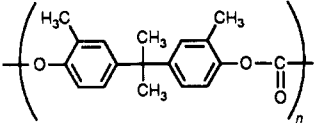
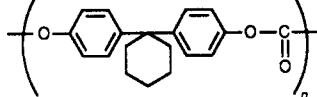
\* To whom correspondence should be addressed. Present address: Reprographic Products Center, Mitsubishi Kasei Corp., Odawara Plant, 1060, Naruta, Odawara, Kanagawa 250, Japan.

**Table I**  
**Structures and Some Properties of Diphenylhydrazone Charge-Transport Molecules (CTM)<sup>a</sup>**

CTM name	structure	formula	formula wt	$\bar{V}_0$ , K, cm <sup>3</sup> /g	$T_g$ , °C	$T_m$ , °C	$T_d$ , °C	cryst density, g/cm <sup>3</sup>	glass density, g/cm <sup>3</sup>	$I_p$ , eV
PY-DPH		C <sub>29</sub> H <sub>20</sub> N <sub>2</sub>	396.5	0.733	42	128	250	1.28	1.20	7.0
CZ-DPH		C <sub>26</sub> H <sub>21</sub> N <sub>3</sub>	375.5	0.748	54	157	250	1.25	1.17	6.8
EA-DPH		C <sub>23</sub> H <sub>25</sub> N <sub>3</sub>	343.5	0.790	16	101	245	1.12	1.09	6.6

<sup>a</sup>  $T_g$  is the glass transition temperature,  $T_m$  the melting point,  $T_d$  the decomposition temperature in air, and  $I_p$  the ionization potential.

**Table II**  
**Repeat Unit Structures and Some Properties of Polycarbonate Binder Resins<sup>a</sup>**

PCR name	structure	repeat unit		$\bar{V}_0$ , K, cm <sup>3</sup> /g	$T_g$ , °C	$T_\beta$ , °C	$T_\gamma$ , °C	glass density, g/cm <sup>3</sup>	$\bar{M}_v \times 10^{-4}$
		formula	formula wt						
A-PCR		C <sub>16</sub> H <sub>14</sub> O <sub>3</sub>	254.3	0.696	150	80	-110	1.198	2.50
C-PCR		C <sub>18</sub> H <sub>18</sub> O <sub>3</sub>	282.4	0.730	124		30	1.160	2.69
Z-PCR		C <sub>19</sub> H <sub>18</sub> O <sub>3</sub>	294.4	0.707	182	80	-70	1.201	3.00

<sup>a</sup> The  $\beta$  dynamic mechanical loss peak is not observed for C-PCR.  $\bar{M}_v$  is the viscosity-average molecular weight.

properties and abrasion, while retaining a common feature in the diphenylhydrazone moiety. Some relevant physical properties are given in Table I. Molecular volume was calculated for the minimum-energy conformation, derived by a semiempirical molecular orbital calculation (MOPAC/AM1). Large single crystals for density measurement were grown from the binary solvent system methylene chloride–1,1,2-trichlorotrifluoroethane.

Three polycarbonates were also chosen for the binder resin. They are BPA-PCR, BPC-PCR, and BPZ-PCR (hereafter abbreviated to A-PCR, C-PCR, and Z-PCR), with quite different glass transition temperatures ( $T_g$ ) and sub- $T_g$  mechanical relaxations, depending on the alkyl substituents at the phenyl ring and isopropylidene bridge. Structures and selected physical properties are shown in Table II. These polymers were obtained from Mitsubishi Gas Chemical Co. The above diphenylhydrazones and polymers are practical materials which have been used in commercial organic photoconductors, and their pairwise combinations provided nine different mixtures for study.

**Sample Preparation.** The polycarbonate and diphenylhydrazone derivative were dissolved separately in tetrahydrofuran (20 and 25 wt %, respectively), and these master batch solutions were passed through a 10- $\mu$ m Millipore filter under pressure to remove traces of dust, which might act as crack nucleation sites

during fracture testing. Afterward, the master batches were intimately mixed to give four different solutions having DPH concentrations equal to 15, 30, 40, and 50 wt % solids (total solid content = 120 g). These solutions were then evaporated in a forced-air oven, with the temperature raised in stages from 60 to 140 °C over a 7-h period. The resulting solid samples are designated PCR/DPH-XY, where PCR type is A, C, or Z, DPH type is PY, CZ, or EA, and XY is the weight percent of DPH (15, 30, 40, or 50).

C-PCR and Z-PCR are amorphous and highly soluble and did not phase separate during solvent evaporation. However, A-PCR had a tendency to crystallize during drying, particularly at high polymer concentration. Complete remixing was ensured by melt compounding (see below). Phase separation of DPH was not a problem, provided its concentration was not too high. However, PY-DPH slowly crystallized if its concentration was 60 wt % or above, so high diluent concentrations in this regime were not studied. Such demixing is not usually a problem for thin films (e.g., 25  $\mu$ m) applied by dip coating to actual photoconductor drums, which dry very rapidly to the frozen glassy state.

Next, the slab of PCR/DPH was cut into pellets, which were ground to less than 2 mm by a Fitz mill. Some solids had high-

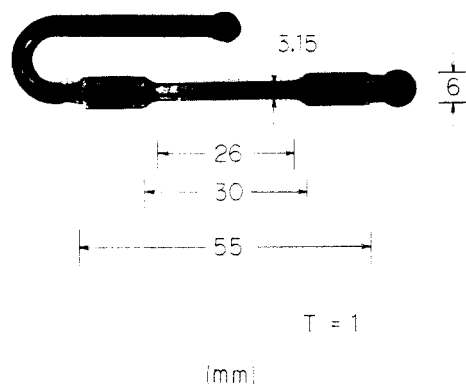


**Figure 1.** Dimensions of an injection-molded tensile test bar as ejected from the mold cavity (runner and sprue also shown). Thickness of bar = 1 mm.

impact toughness, which necessitated cooling with liquid nitrogen before grinding. The powders so obtained were vacuum dried for about 18 h just below  $T_g$  to eliminate traces of solvent and absorbed water and fed into a single-screw injection-molding machine (Japan Steel Works, Model J5S, 0.1 oz.) to fabricate tensile test bars. Injection molding was superior to melt pressing and solvent casting for obtaining large, uniform samples that were dry and free from voids.

The ASTM standard test bar (ASTM D 638-86) was not prepared because material was limited. Instead, a smaller test bar that weighed about 0.29 g was used. Its dimensions are shown in Figure 1. At least 10 test bars were molded for each composition, requiring about 50 g of material in total (flushing the screw and barrel assembly at each changeover in composition created much waste). The mold cavity was maintained at room temperature, and no release agent which might induce stress cracking was used. There were practical limits to the concentration of the PCR diluent (DPH). The lower limit was 15 wt %, below which melt viscosity was too high for injection below the thermal decomposition temperature of DPH at 250 °C (see below). The upper limit was 50 wt %, above which test bars were too brittle to withstand ejection from the mold.

The temperature of the injection barrel and screw assembly was carefully chosen to achieve a melt viscosity suitable for proper mold fill (generally from 700 to 8000 P at a shear rate of 1000  $s^{-1}$ ). A Shimadzu flow tester (0.1  $\times$  1 cm die) was used to determine this temperature, by recording the melt viscosity at various shear rates. Samples with 50 wt % DPH had a low viscosity and could be injected readily from 160 to 180 °C. However, elevated temperatures were necessary for samples with a lower DPH concentration, owing to their increased melt viscosity. The maximum safe temperature of the injection barrel was around 220 °C, above which autooxidation of DPH became a problem (shear heating by the screw increased the temperature by about 20 °C). Concentrated PCR compositions with less than 15 wt % DPH were usually too viscous for molding below the DPH decomposition temperature. Oxidized test bars were noticeably darker in color and fractured at lower stress. To prevent autooxidation, nitrogen gas was supplied to the sample inlet as needed. Undiluted PCR resins were thermally much more stable and were molded from 280 to 340 °C with no problem.

**Thermal Analysis and Density.** Thermal gravimetric analysis (TGA) was used to determine the onset of thermal decomposition ( $T_d$ ) in air, at a heating rate of 20 °C·min $^{-1}$ .  $T_g$  values (and  $T_m$  = melting point, where applicable) were recorded by differential scanning calorimetry (DSC) at 10 °C·min $^{-1}$ .  $T_g$  was determined for thermally annealed PCR/DPH mixtures as the first inflection point during heating, and  $T_m$  was taken as the maximum endotherm position. Crystalline DPH was first melted and then rapidly quenched to -80 °C to form the amorphous (glassy) phase. Both TGA and DSC were recorded with ULVAC Sinku-Riko instruments (Models TGD 7000 and DSC 7000, respectively). Some samples had poorly resolved, broad  $T_g$  by DSC, and DMA (see below) gave a more reliable measurement. The densities of molded samples were measured in a density-gradient column at 23 °C.

**Tensile Test and Aging.** An Intesco Model 2005 tensile tester was used to record the extensional stress-strain (force-deformation) curves of the injection-molded test bars at ambient temperature. Tensile bars were extended to the point of break in the longitudinal direction, after being aged for 1 week at room temperature. Transverse properties were not determined. At least five bars were measured at each composition, and the results, averaged. The reproducibility of tensile strength and modulus values was usually within 10%, but the extension to break for ductile samples was not as consistent. The crosshead speed was 5 mm·min $^{-1}$ , corresponding to an initial strain rate of  $2.78 \times 10^{-3}$  s $^{-1}$ . Young's modulus was calculated from the initial slope from 0 to 1% strain.

Test bars were anisotropic, with partial orientation (alignment) and extension of polymer chains in the longitudinal (injection flow) direction. This orientation was not fully relaxed during the rapid quench to room temperature in the mold cavity. The properties of PCR are known to change with time due to aging. This aging phenomenon usually results in densification (relaxation of excess free volume), accompanied by an increase in brittleness. Partial relaxation of internal stress was possible by annealing near the glass transition temperature for a sufficiently long period. However, different PCR/DPH combinations and compositions have different relaxation rates, so it was not practical to ensure uniform aging, let alone determine the extent of relaxation. In any case, it is doubtful that the equilibrium state could be achieved. For this reason, all samples were tested with an identical history as described above, to establish a consistent basis for comparing their relative behavior.

**Dynamic Mechanical Analysis.** Dynamic mechanical analysis (DMA) was performed from -150 to about +15 °C above  $T_g$  at a heating rate of 1.5 °C·min $^{-1}$  with a Du Pont 983 instrument operating in the oscillating forced flexural mode (amplitude 0.2 mm), at a fixed frequency of 1 Hz. This frequency was chosen because of its close match to the actual copy machine process speed. The solid sample was an injection-molded bar, 7 mm wide and 3 mm thick, with a length between clamps of 18 mm.  $T_g$  was assigned to the maximum position of the  $\alpha$  peak in the loss modulus ( $G''$ ) curve. The reproducibility of DMA data was excellent.

**Taber Film Abrasion Test.** PCR/DPH mixtures in a methylene chloride solution were draw-bar-coated on a 100- $\mu$ m aluminized polyester sheet, to provide a solid film having a thickness of 35  $\mu$ m after drying, and 120-mm-diameter circles were cut out for abrasion testing. A Taber-type abrader was used (manufactured by Toyoseiki Co.), utilizing two Kent paper-covered abrasive disks with a 250-g load, according to industrial standard JIS K7204 (1977). One abrasion cycle consisted of a complete rotation of a circular turntable supporting the test sheet, so that the abrasive disks covered a wear track 27 mm wide and a 90-mm outer diameter on the surface of the PCR/DPH film. The sheet temperature was maintained at 20 °C, and wear debris was constantly removed by suction. The film weight loss was essentially linear with the number of cycles and was recorded at 1000-cycle intervals up to a total of 5000 cycles. Three separate sheets were tested at each composition, and the results were then averaged.

## Results and Discussion

**Thermal Analysis.** TGA showed that the onset of autooxidation of all DPH derivatives is from 245 to 250 °C. The most labile structure is the hydrazone double bond. This  $T_d$  value is hardly affected by the molecular dispersion of DPH in PCR. The practical significance of  $T_d$  is that it set the upper limit on the injection-molding temperature.

Melt rheological data exhibited the expected non-Newtonian behavior, with viscosity decreasing from about 10 000 to 1000 P as the shear rate increased from 100 to 1500  $s^{-1}$ . The neat PCR have melt viscosities increasing in the order C < A < Z at a given temperature and shear rate. Since their molecular weights are comparable, this sequence follows the same trend as  $T_g$  (Table II), reflecting the increasing barrier to rotational reorientation (stiffness)

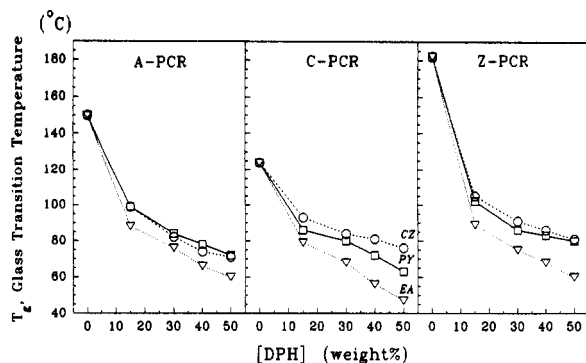


**Figure 2.** Glass transition temperatures of solid PCR/DPH mixtures as a function of composition and diphenylhydrazone (PCR diluent) concentration. DPH type: PY-DPH ( $\square$ ), CZ-DPH ( $\circ$ ), EA-DPH ( $\nabla$ ).

along the polymer backbone. Dilution of PCR by DPH reduced viscosity strongly, allowing lower temperatures to be used for injection molding of mixtures. In this sense, DPH may be thought of as a "solvent" for PCR. Other factors being equal, EA-DPH gave the lowest viscosity mixtures, and PY-DPH, the highest.

$T_g$  of the PCR is always significantly higher than that of the DPH derivatives and decreases in the order  $Z > A > C$  for PCR and  $CZ > PY > EA$  for DPH (Tables II and I, respectively). Therefore,  $T_g$  of the mixture decreases with increasing concentration of the lower- $T_g$  diluent (DPH), as shown in Figure 2. In the concentration range suitable for efficient charge transport in a practical organic photoconductor, typically around 50 wt % DPH,  $T_g$  of a PCR/DPH mixture depends more on the choice of DPH structure than PCR. Hence DPH with low  $T_g$  like EA-DPH are disadvantageous, since they depress the  $T_g$  of their mixtures with PCR close to room temperature. Then surface damage by frictional heating and scratching may be more likely under actual service conditions.

Often,  $T_g$  values of polymer-diluent systems are described by the monotonic Gordon-Taylor expression

$$T_g = \frac{kW_1(T_g)_1 + (1 - W_1)(T_g)_2}{kW_1 + (1 - W_1)} \quad (1)$$

where  $W_1$  is the weight fraction of the diluent,  $(T_g)_2$  is the  $T_g$  of the polymer, and  $k$  is an adjustable parameter ( $k > 0$ ) equal to the ratio of free-volume expansion coefficients of diluent to polymer. In the present case, eq 1 gives a poor fit to the data, with  $k$  values from 2.8 to 6.2 and standard deviations as high as 15%.

More recently, Scandola et al.<sup>9</sup> find two  $T_g$  regimes for polymer-diluent mixtures, corresponding to the polymer-rich regime and the diluent-rich regime. Such behavior is shown also by the data in Figure 2, with a discontinuity (or cusp) in the curves for DPH concentration around 35 wt %. The glass transition becomes broad and indistinct in the regime transition zone (even two  $T_g$  may be observed), which accounts for the occasional difficulty experienced in discerning  $T_g$  by DSC. All samples prepared in this work are optically clear, suggesting that the solid phase is homogeneous, at least on the order of the wavelength of visible light. Therefore, macrophase separation is not responsible for the  $T_g$  behavior.

**Density and Free Volume.** The densities of injection-molded PCR/DPH mixtures are shown in Figure 3.

The ideal law of mixing assumes volume additivity

$$\hat{V}_i = W_1\hat{V}_1 + (1 - W_1)\hat{V}_2 \quad (2)$$

where  $\hat{V}_i$  is the ideal specific volume (inverse density in  $\text{cm}^3\text{-g}^{-1}$ ) and  $W_1$  is the weight fraction of DPH. All PCR/

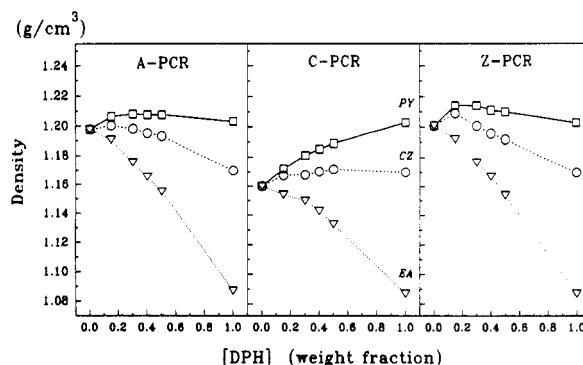


**Figure 3.** Densities of solid PCR/DPH mixtures as a function of composition and DPH concentration. DPH type: PY-DPH ( $\square$ ), CZ-DPH ( $\circ$ ), EA-DPH ( $\nabla$ ).

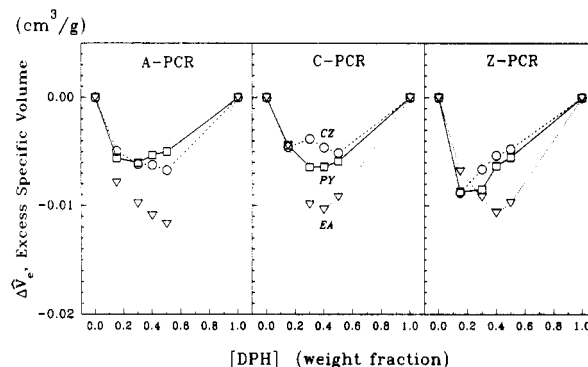


**Figure 4.** Negative deviation of excess specific volumes from ideal mixing as a function of composition and DPH concentration. DPH type: PY-DPH ( $\square$ ), CZ-DPH ( $\circ$ ), EA-DPH ( $\nabla$ ).

DPH mixtures exhibited nonideal behavior, with negative excess specific volumes, calculated according to

$$\Delta\hat{V}_e = \hat{V} - \hat{V}_i \quad (3)$$

where  $\hat{V}$  is the actual specific volume of the mixture.<sup>10</sup> The deviation from ideal mixing is shown in Figure 4. This negative deviation is usual for polymers diluted by small molecules, as well as for blends of two compatible polymers.<sup>11</sup> It results from the stronger attraction between unlike molecules, which gives rise to miscibility or compatibility. However, it should be emphasized that the glassy state of injection-molded PCR/DPH mixtures is not at equilibrium, so that a thermodynamic analysis of mixing cannot be applied to these data.

Mixtures with the highest absolute densities are obtained from Z/PY combinations, and the lowest densities result from C/EA mixtures, as expected from the densities of pure components (Tables I and II). The largest deviation from ideal mixing is obtained with EA-DPH. This may be interpreted in two ways. Either EA-DPH has the strongest attraction to PCR compared to the other DPH derivatives or its low  $T_g$  value and internal flexibility (from the diethylamine group) allow the mixture with PCR to relax (age) more fully after molding to the densified state. Hole transport molecules must be electron donors, and EA-DPH has the lowest ionization potential of the DPH derivatives studied here (Table I). The carbonyl group of PCR is a weak electron acceptor, so it is reasonable that EA-DPH may have the strongest charge-transfer interaction with PCR compared to PY-DPH and CZ-DPH.

Specific free volumes were derived from the equation

$$\hat{V}_F = \hat{V} - \hat{V}_{0K} \quad (4)$$

where  $\hat{V}_F$  is the specific free volume in  $\text{cm}^3\text{-g}^{-1}$  and  $\hat{V}_{0K}$  is the zero point specific volume.<sup>10,12</sup> The latter is related

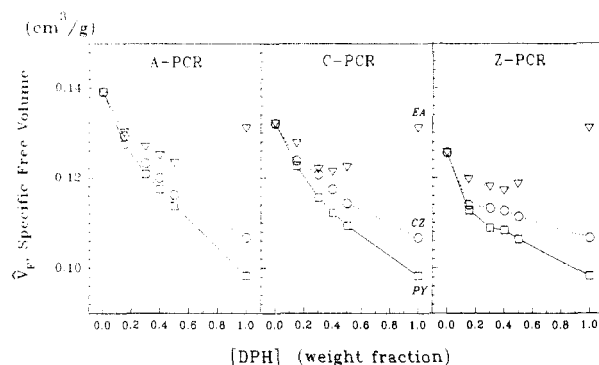


**Figure 5.** Specific free volumes of solid PCR/DPH mixtures. DPH type: PY-DPH ( $\square$ ), CZ-DPH ( $\circ$ ), EA-DPH ( $\nabla$ ).

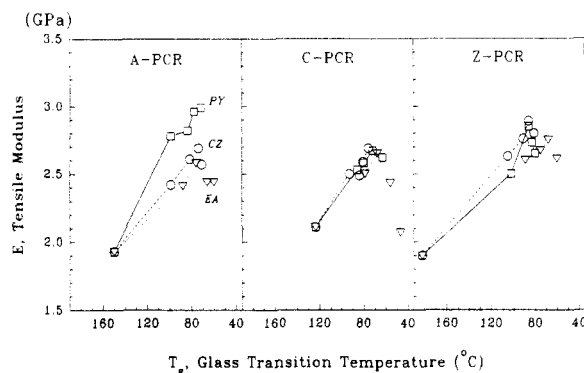


**Figure 6.** Variation of the tensile modulus with the composition and glass transition temperature of PCR/DPH mixtures. All samples are antiplasticized, except for C/EA-50. DPH type: PY-DPH ( $\square$ ), CZ-DPH ( $\circ$ ), EA-DPH ( $\nabla$ ).

to the van der Waals specific volume  $\hat{V}_W$  by

$$\hat{V}_{0K} = 1.3\hat{V}_W \quad (5)$$

$\hat{V}_W$  for DPH molecules were calculated by a molecular simulation program, and  $\hat{V}_{0K}$  values (Table I) were derived from eq 5.  $\hat{V}_{0K}$  for the various PCR (Table II) were taken from the literature.<sup>13</sup>

$\hat{V}_F$  data as a function of structure and composition are shown in Figure 5. Free volume decreases in the order  $A > C > Z$  for PCR and  $EA > CZ > PY$  for DPH. Concerning the polymer-diluent mixtures, the free volume of PCR is reduced by addition of DPH. This reduction in free volume has been reported for many other polymer systems diluted by small-molecule additives. It is thought that the diluent at first fills the available free volume, although the average free volume cavity in A-PCR is about  $0.165 \text{ nm}^3$ , which is too small to accommodate bulky DPH molecules (Table I) without distortion of the surrounding lattice.

The fractional free volume in the amorphous solid state of DPH is less than that in PCR, because of denser packing. PY-DPH has the lowest glassy free volume, and EA-DPH, the highest. The same trend in packing efficiency exists in the crystalline state of DPH derivatives (densities in Table I). Therefore, the general trend shown in Figure 5 is reasonable, particularly if the forces between PCR and DPH are attractive, as suggested by the  $\hat{V}_e$  values. As expected, Z/PY mixtures which have the highest densities have the lowest free volumes.

**Tensile Elongation to Break.** Tensile testing revealed that DPH additives cause significant antiplasticization of PCR. This is apparent from Figure 6, which shows that a decrease in  $T_g$  is accompanied by an increase in the modulus  $E$ . Such a decrease in  $T_g$  results from enhanced long-range segmental mobility and is the normal result of plasticization, but when combined with a stiffening of the

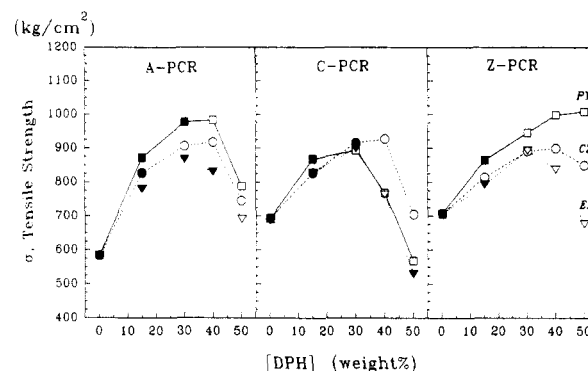


**Figure 7.** Tensile strength at yield (ductile samples, filled points) or break (brittle samples, open points) as a function of composition and DPH concentration. DPH type: PY-DPH ( $\square$ ), CZ-DPH ( $\circ$ ), EA-DPH ( $\nabla$ ).

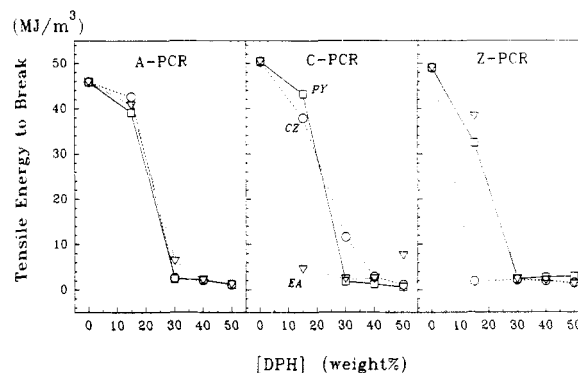


**Figure 8.** Tensile energy to break showing the transition from ductile to brittle behavior as DPH concentration is increased. DPH type: = PY-DPH ( $\square$ ), CZ-DPH ( $\circ$ ), EA-DPH ( $\nabla$ ).

glassy phase (increased modulus, brittleness), the effect is then known as antiplasticization. This opposite effect on viscoelastic properties above and below  $T_g$  is a characteristic feature of an antiplasticized system.<sup>14</sup>

Figure 7 shows the trend in the tensile strength as a function of DPH concentration. Tensile strength also increases due to antiplasticization and becomes maximum from 35 to 50 wt % DPH. Strictly speaking, the terms "plasticization" and "antiplasticization" are inappropriate at high diluent concentrations, as these concepts are meaningful only in the context of a polymer-rich matrix.

The fracture behavior of neat PCR can be either ductile or brittle, depending on variables such as thickness, deformation rate, temperature, orientation, physical aging, and molecular weight. This response has been termed pseudoductile.<sup>15</sup> Under present conditions, three modes of failure were observed, depending on DPH concentration: (i) ductile, (ii) intermediate crazing, and (iii) crack regimes. Undiluted polymers were ductile and failed after yielding, necking, and drawing at ultimate extensions of 83%, 72%, and 68% for A-PCR, C-PCR, and Z-PCR, respectively. Also, PCR/DPH mixtures were ductile at the lowest DPH concentration of 15 wt % but became brittle (crazing, later developing into major crack failure) as more DPH was added. Z-PCR was the most sensitive to embrittlement by DPH, and A-PCR was the least sensitive.

The tensile energy to break is plotted in Figure 8. The tensile energy to break is obtained from the area under the stress-strain curve, and it decreases dramatically for brittle samples, which typically fail at extensions around 4%. The one mixture that was not antiplasticized was C/EA-50, which was ductile with 33% extension to break and had a modulus less than that of neat C-PCR (Figure 6). Interestingly, this sample, as well as some other ductile compositions, embrittled after prolonged aging at room

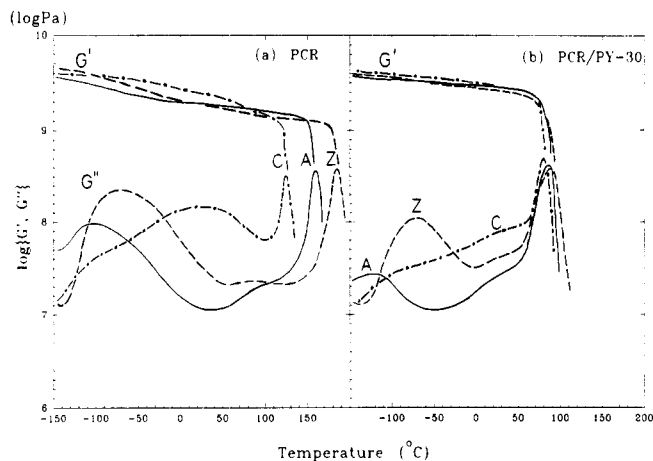


**Figure 9.** Dynamic mechanical storage ( $G'$ ) and loss ( $G''$ ) moduli at 1 Hz for (a) pure polycarbonate binder resins and (b) the same resins diluted with 30 wt % PY-DPH.

temperature (130 days). A discussion of such long-term aging is beyond the scope of the present paper.

**Dynamic Mechanical Analysis.** DMA measurements were made to probe the effect of DPH addition on internal motions which give rise to mechanical relaxations in the glassy phase of PCR. Figure 9 shows the storage and loss moduli (real and imaginary components, respectively, of the complex viscoelastic modulus  $G^*$ ) for (a) undiluted PCR and (b) the same polymers containing 30 wt % PY-DPH. The storage or elastic modulus  $G'$  is equivalent to Young's modulus  $E$  already determined at room temperature by the tensile test. DMA provides the temperature dependence of  $G'$ , which has a strong inflection at  $T_g$ , and increases slightly with decreasing temperature below  $T_g$ . More attention will be focused on the loss modulus  $G''$  in this section.

There are usually three mechanical loss peaks observed for PCR.<sup>16</sup> The primary relaxation ( $\alpha$  peak) occurs at highest temperature and results from long-range segmental motion at  $T_g$ . The aromatic methyl substituents in C-PCR evidently inhibit tight chain packing compared to the unsubstituted A-PCR, accounting for the lower density and  $T_g$ . However, the cyclohexyl substituent in Z-PCR apparently stiffens the chain backbone and results in a higher  $T_g$ . Molecular interpretation of such substituent effects on PCR  $T_g$  has been given by Yee and Smith.<sup>16</sup>

The two secondary (sub- $T_g$ ) relaxations are the  $\beta$  and  $\gamma$  peaks, in order of decreasing temperature. Their positions are summarized in Table II. The minor  $\beta$  peak is thought to result from orientational stress and excess free volume in the material (packing defects),<sup>17</sup> and it may not be observed if the  $\alpha$  and  $\gamma$  peaks are close together, as in C-PCR. It can be reduced in intensity or even eliminated by thermal aging or solvent casting. The most interesting peak from the point of view of this work is the low-temperature  $\gamma$  relaxation, which moves to higher temperatures as the PCR backbone is substituted with bulky groups that hinder motion.

DPH addition causes several significant changes. The position, but not intensity, of the  $\alpha$  peak changes as  $T_g$  is reduced by dilution of PCR with the DPH derivative. C-PCR is an interesting case in that its  $\alpha$  and  $\gamma$  peaks begin to overlap. The weak  $\beta$  peak gradually disappears as DPH concentration increases, probably due to the relaxation of orientational stress with a corresponding reduction in free volume. DPH molecules may act as an "internal solvent" and facilitate this process. A common feature is the reduction in the intensity and width of the  $\gamma$  peak, although the maximum position is hardly affected.

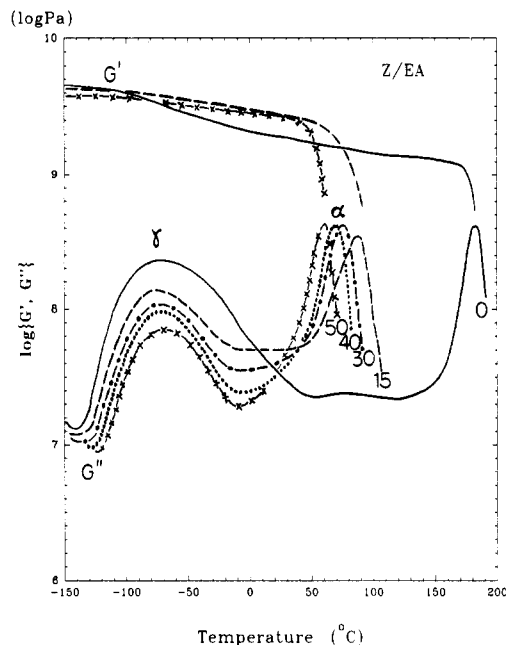


**Figure 10.** Effect of increasing EA-DPH concentration on the dynamic mechanical storage and loss moduli of Z-PCR (not all storage modulus curves are shown for clarity).

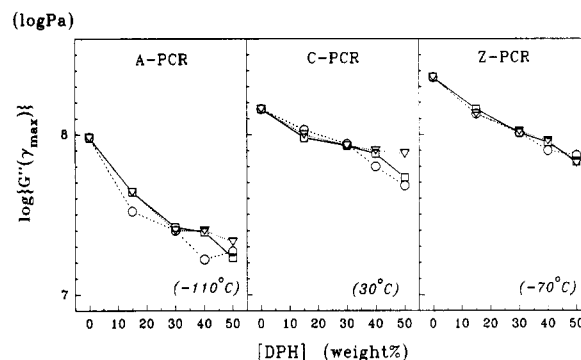


**Figure 11.** Suppression of the intensity of the dynamic mechanical  $\gamma$  peak maximum (at indicated temperatures) by DPH. DPH type: PY-DPH ( $\square$ ), CZ-DPH ( $\circ$ ), EA-DPH ( $\nabla$ ).

Figure 10 shows this trend in more detail for the full range of DPH concentrations, taking Z/EA mixtures as representative examples. The four notable effects of antiplasticization on  $G^*$  are clearly illustrated. They are as follows: (i) an increase in the elastic or storage modulus  $G'$ ; (ii)  $\alpha$  peak shift—the maximum position of  $G''$  is shifted to lower temperatures; (iii)  $\gamma$  peak suppression— $G''$  is reduced in intensity (peak at  $-70^\circ\text{C}$ ); and (iv) narrowing of  $\gamma$  peak width, particularly on the high-temperature side.

The reduction in intensity of the  $\gamma$  peak maximum for all PCR/DPH mixtures and concentrations is shown graphically in Figure 11. The magnitude and sensitivity of this peak to antiplasticization depends mostly on the PCR structure, with all DPH types having a similar effect. The intensity of the  $\gamma$  loss peak, as indicated by the  $G''$  value at the peak maximum, decreases in the order Z-PCR > C-PCR > A-PCR for the neat polymers, as well as for diluted mixtures at a given DPH concentration. A-PCR has the lowest temperature  $\gamma$  peak, and this shows the strongest suppression after DPH addition.

**Relation between Moduli and Free Volume.** There is a general correlation between the  $\gamma$  mechanical loss modulus and free volume. This is shown in Figure 12. A small decrease in free volume is accompanied by a significant reduction in  $G''$ , perhaps because of the restricted freedom for large-amplitude oscillations of

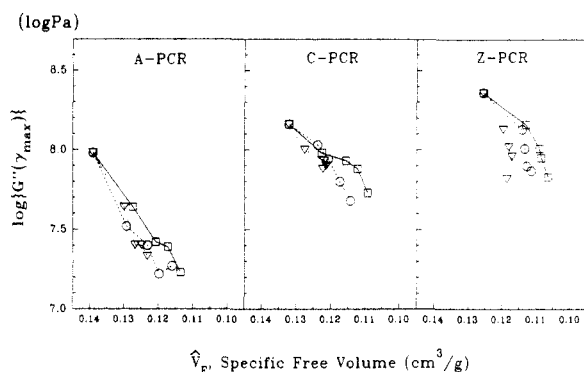


**Figure 12.** Correlation between the intensity of the dynamic mechanical  $\gamma$  peak and the specific free volume of PCR/DPH mixtures. DPH type: PY-DPH ( $\square$ ), CZ-DPH ( $\circ$ ), EA-DPH ( $\nabla$ ).

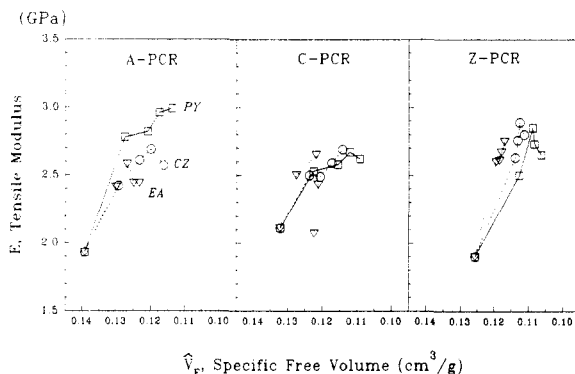


**Figure 13.** Correlation between tensile modulus  $E$  and the specific free volume of PCR/DPH mixtures. Sample C/EA-50 shows strong deviation due to plasticization. DPH type: PY-DPH ( $\square$ ), CZ-DPH ( $\circ$ ), EA-DPH ( $\nabla$ ).

polymer segments that absorb mechanical energy in the glassy phase.

Figure 13 shows that there is also a correlation between the elastic modulus  $E$  measured by the tensile test and free volume. Not surprisingly, the stiffness of the PCR/DPH glassy matrix increases as the free volume is reduced. Sample C/EA-50 is a striking exception, because it is plasticized, and the significance of this is discussed in the next section.

Although the correlations in Figures 12 and 13 are at least indicative of some connection between mechanical properties and internal structure, it is rather simplistic to expect a linear dependence of modulus on free volume. For example, the extent of dynamic mechanical loss is given by the total area under the loss peak and not just the maximum value of  $G''$ . For the reasons discussed below, this area was difficult to determine.

**Antiplasticization and Molecular Motion.** The relation between antiplasticization of PCR by diluents and mechanical loss is still the subject of much active research, and the exact molecular origin of the  $\gamma$  relaxation is not firmly established yet. Although small-molecule diluents reduce free volume, their effect on dynamics is perhaps more significant. It is generally agreed that the  $\gamma$  peak in PCR is related to local free-volume fluctuation (lattice breathing) from intermolecularly coupled oscillations of polymer main-chain segments.<sup>18,19</sup> These motions are dynamically heterogeneous, with a broad and asymmetric distribution of frequencies. Solid-state NMR studies have indicated that addition of diluent to PCR suppresses free-volume fluctuation, with a narrowing of the frequency distribution and reduction in amplitude of short-range segmental oscillations thought to accompany the low-temperature mechanical loss.<sup>20-22</sup> Some site-

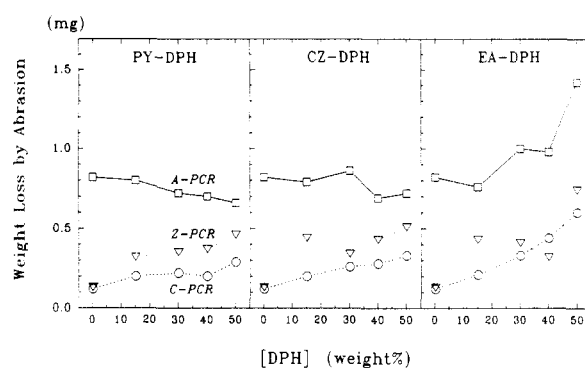


**Figure 14.** Dependence of abrasion loss of PCR/DPH mixtures as a 35- $\mu\text{m}$ -thick film on DPH structure and concentration. PCR type: C-PCR ( $\circ$ ), A-PCR ( $\square$ ), Z-PCR ( $\nabla$ ).

specific interaction between PCR and diluent has also been suggested. Moreover, it is well established that the phenyl rings in PCR undergo rapid 180° flips in the glassy matrix and that these flips correlate with local free-volume fluctuation.<sup>18</sup>

Jho and Yee<sup>23</sup> reported a key finding from their study of block copolycarbonates with widely separated  $\gamma$  peaks and carefully controlled block lengths. They found that the shortest "mechanically active" segment is about 9 monomer repeat units, corresponding to the average distance between chain entanglement points, which act as nodes in the short-range segmental oscillations. A recent molecular dynamics simulation of PCR by Suter et al.<sup>24</sup> highlights the long-range intermolecular cooperativity of such motion. Their paper also gives a detailed summary of the existing literature on PCR dynamics.

A different mechanism for  $\gamma$  relaxation involves independent motion of substituents adjacent to the main chain; such motion of pendant substituents is not considered "mechanically active". A present example is the chair-chair conformational flip of the cyclohexyl group in Z-PCR, which has a relaxation maximum around -90 °C at 1 Hz.<sup>25</sup> This combines with the main-chain  $\gamma$  peak at -70 °C, so the strong  $\gamma$  peak of Z-PCR is in reality a superposition of two internal relaxation modes, which may have different sensitivities to antiplasticization. In the case of C-PCR, the  $\gamma$  peak intensity has a contribution from the shifted  $\alpha$  peak at high DPH diluent concentration, so both short-range and long-range segmental motions are involved. For these reasons, it was not possible to accurately measure the actual area of the dynamic mechanical loss peak. To a first approximation, all PCR studied here have similar types of main-chain oscillation, although with different frequencies and activation energies.<sup>26</sup>

**Surface Abrasion of Film.** It is instructive to group the abrasion data by DPH additive type, rather than by PCR type. The results are shown in Figure 14. Weight loss of A-PCR is significantly higher than either Z-PCR or C-PCR. Perhaps the most interesting feature is the effect of increasing DPH concentration on abrasion. Abrasion increases for C-PCR and Z-PCR, as to be expected as the polymer entanglement density is reduced by the small-molecule diluent, but surprisingly decreases somewhat for A-PCR.

Abrasion of polymers is a highly complex and poorly understood phenomenon, involving both surface and bulk properties. Generally, at least two basic kinds of abrasion mechanisms are postulated: scratch (penetration and plowing of the polymer matrix by a hard asperity) and fatigue (gradual loss of the entire surface layer by repetitive cyclic loading under adhesive contact). Of course, under the actual service conditions of an organic photoconduc-



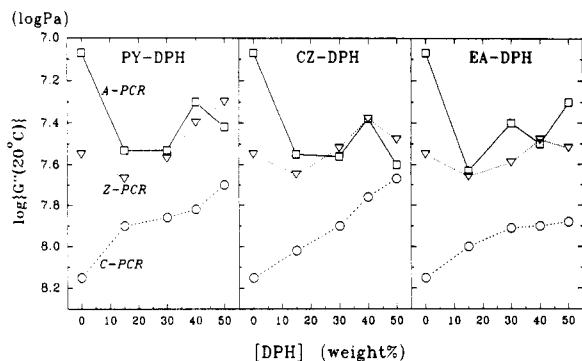


**Figure 15.** Effect of DPH structure and concentration on the dynamic mechanical loss modulus at 20 °C. PCR type: C-PCR (○), A-PCR (□), Z-PCR (▽).

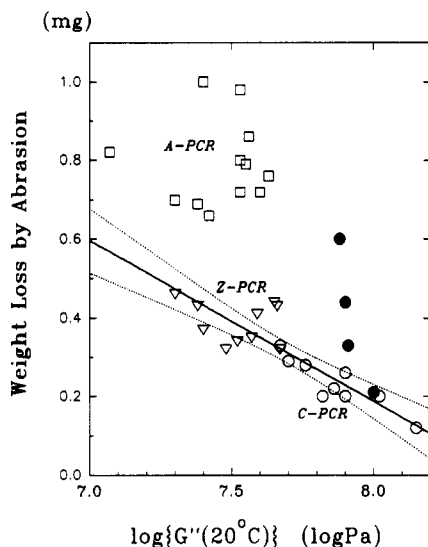


**Figure 16.** Correlation between abrasion loss of PCR/DPH films and loss modulus at test temperature (20 °C). Linear least-squares fits to data for C-PCR and Z-PCR (with 95% confidence limits) are shown. Abrasion data for A-PCR (open squares) and C/EA mixtures (filled circles) do not fit the correlation. PCR type: C-PCR (○), A-PCR (□), Z-PCR (▽). C/EA formulations: ●.

tor, there is a contribution from several types of abrasion mechanisms. For the present discussion, it is assumed that abrasion by paper predominantly involves the fatigue mechanism. Furthermore, it is proposed that this may be reduced by the absorption and dissipation of external stress as internal heat, which can quickly and harmlessly diffuse through the thin charge-transport layer into the aluminum substrate, provided there is efficient coupling to a mechanical loss process at the temperature of test. Otherwise, mechanical stress remains concentrated at the surface, with the likelihood of increased abrasion.

The effect of the structure and composition of PCR/DPH mixtures on the loss modulus at 20 °C is plotted in Figure 15. C-PCR and Z-PCR exhibit the *opposite* trend compared to A-PCR for increasing DPH concentration, as was also the case for abrasion. It therefore appears plausible that some correlation exists between abrasion and the dynamic mechanical loss modulus, at least amongst the closely related materials tested here.

The correlation is shown in Figure 16, where there is a universal trend of abrasion rate decreasing as the loss modulus increases. The correlation appears reasonable, given the rather naive assumption that abrasion is related to one single material parameter. However, there are significant deviations that expose the weakness of the above assumption. They are exhibited by all materials

prepared with A-PCR binder resin and combinations of C-PCR with EA-DPH, which have higher abrasion rates than expected.

In the case of A-PCR, the  $\gamma$  loss process is well below room temperature (Figure 9), so that the loss modulus at 20 °C has a negligible contribution from the mechanically active free-volume fluctuations thought to be important for toughness. Z-PCR is an intermediate case. In contrast, C-PCR and its mixtures with DPH diluents have a  $\gamma$  mechanical loss process centered at the abrasion test temperature. This would appear to be the optimum condition. However, C/EA mixtures are an anomaly, because of plasticization and ductility. Clearly factors additional to the loss modulus influence abrasion, and ductility would appear to be detrimental to material durability.

Dilution by EA-DPH resulted in the highest abrasion rate, largest free volume, largest deviation from ideal mixing, as well as the lowest melt viscosity, lowest  $T_g$ , and lowest density, as described above. This particular DPH derivative, when mixed with C-PCR in equal parts by weight, gave a plasticized and ductile solid with enough internal motion to cause appreciable long-term aging at room temperature. In this regard, it is significant that, of the three DPH studied, only EA-DPH has a  $T_g$  below room temperature and the  $\gamma$  peak maximum of C-PCR. Whether plasticization or antiplasticization results at a particular temperature therefore depends to a large degree on the relative mobility of the diluent and polymer in the glassy phase.<sup>27,28</sup>

It is believed that two motionally distinct populations of diluent molecules exist in polymer glasses. At low concentrations, the diluent is supposed to be associated with polymer segments, much like a solvation shell, and to have restricted motion. At higher concentrations (e.g., above 30 wt %), diluent pairwise contacts are more probable, and microscopic clusters of mobile diluent are supposed to form,<sup>6,22</sup> without actual macroscopic phase separation taking place. If this is the case for DPH derivatives, EA-DPH molecules in amorphous clusters would have liquidlike mobility at room temperature and contribute to plasticization and poor abrasion resistance.

## Conclusions

The antiplasticization of PCR by small-molecule diluents depends on the host polymer structure, concentration, deformation rate, and temperature. In an antiplasticized system, the effect of diluent molecules may be considered from both static and dynamic viewpoints. They reduce local free-volume size and oscillation amplitude and result in increased strength and elastic modulus, as well as embrittlement by stress concentration. However, a diluent is not intrinsically an antiplasticizer or plasticizer, and the concept is relevant only in the context of a polymer-diluent system under specified conditions. It is thought that antiplasticization is possible only for polymers having mechanically active main-chain motions below  $T_g$ . Polycarbonate is perhaps the best known example.

The abrasion resistance of the charge-transport layer of organic photoconductors, consisting of diphenylhydrazone derivatives molecularly dispersed in a glassy PCR matrix, depends on several material properties. The addition of low molecular weight charge-transport molecules dilutes the PCR entanglement density, which should allow easier chain slippage under frictional stress and cause dramatically increased wear. That this is not the case may be attributed to antiplasticization. Loss of free volume and the hindrance of short-range segmental oscillations implicated in the mechanical loss process by a less mobile



diluent contribute to a stiff polymer matrix. A possible interpretation of abrasion resistance is given in terms of the dynamic mechanical loss modulus, although other material properties are involved as well.

A durable charge-transport layer for organic photoconductors should incorporate a binder resin that has a broad and intense sub- $T_g$  mechanical loss process involving backbone segmental motion. The temperature dependence of the loss is important, and the optimum condition may be obtained when the loss peak maximum matches the desired service temperature of the photoconductor. Finally, a charge-transport molecule that causes antiplasticization should be incorporated. PCR are perhaps the most suitable class of polymers fulfilling these requirements, and it is interesting that they found commercial application in organic photoconductors before the relevance of the above dynamic mechanical attributes was fully appreciated. There is still scope for improving the resistance of PCR to fatigue abrasion by broadening the  $\gamma$  relaxation and shifting its maximum position to a higher temperature. This may be done by the judicious choice of backbone substituents and copolymerization, and work in this direction is currently in progress.

**Acknowledgment.** We thank Dr. S. Shimizu for the use of DMA equipment, Mr. H. Takeuchi for computations of the molecular structure of DPH derivatives, and Mr. O. Ando for DSC measurements.

## References and Notes

- (1) Schein, L. B. *Electrophotography and Development Physics*; Springer Series in Electrophysics 14; Springer-Verlag: Berlin, 1988.
- (2) Conix, A.; Jeurissen, L. *Adv. Chem. Ser.* **1965**, *48*, 172.
- (3) Jackson, W. J.; Caldwell, J. R. *Adv. Chem. Ser.* **1965**, *48*, 185.
- (4) Jackson, W. J.; Caldwell, J. R. *J. Appl. Polym. Sci.* **1967**, *11*, 211.
- (5) Ngai, K. L.; Rendell, R. W.; Yee, A. F.; Plazek, D. J. *Macromolecules* **1991**, *24*, 61.
- (6) Jones, A. A.; Inglefield, P. T.; Liu, Y.; Roy, A. K.; Cauley, B. J. *J. Non-Cryst. Solids* **1991**, *131-133*, 556.
- (7) Pochan, J. M.; Hinman, D. F.; Turner, S. R. *J. Appl. Phys.* **1976**, *47*, 4245.
- (8) Pochan, J. M.; Pochan, D. F. *Polymer* **1991**, *32*, 2238.
- (9) Scandola, M.; Ceccorulli, G.; Pizzoli, M. *Polymer* **1987**, *28*, 2081.
- (10) Maeda, Y.; Paul, D. R. *J. Polym. Sci., Part B: Polym. Phys.* **1987**, *25*, 1005.
- (11) Yee, A. F. *Polym. Eng. Sci.* **1977**, *17*, 213.
- (12) Lee, W. M. *Polym. Eng. Sci.* **1980**, *20*, 65.
- (13) Schmidhauser, J. C.; Longley, K. L. *J. Appl. Polym. Sci.* **1990**, *39*, 2083.
- (14) Kambour, R. P.; Kelly, J. M.; McKinley, B. J. *J. Polym. Sci., Part B: Polym. Phys.* **1989**, *27*, 1979.
- (15) Chang, F.-C.; Hsu, H.-C. *J. Appl. Polym. Sci.* **1991**, *43*, 1025.
- (16) Yee, A. F.; Smith, S. A. *Macromolecules* **1981**, *14*, 54.
- (17) McHattie, J. S.; Koros, W. J.; Paul, D. R. *J. Polym. Sci., Part B: Polym. Phys.* **1991**, *29*, 731.
- (18) Schaefer, J.; Stejskal, E. O.; Perchak, D.; Skolnick, J.; Yaris, R. *Macromolecules* **1985**, *18*, 368.
- (19) Fischer, E. W.; Hellmann, G. P.; Spiess, H. W.; Horth, F. J.; Ecarius, E.; Wehrle, M. *Makromol. Chem. Suppl.* **1985**, *12*, 189.
- (20) Poliks, M. D.; Gullion, T.; Schaefer, J. *Macromolecules* **1990**, *23*, 2678.
- (21) Belfiore, L. A.; Henrichs, P. M.; Massa, D. J.; Zumbulyadis, N.; Rothwell, W. P.; Cooper, S. L. *Macromolecules* **1983**, *16*, 1744.
- (22) Liu, Y.; Roy, A. K.; Jones, A. A.; Inglefield, P. T.; Ogden, P. *Macromolecules* **1990**, *23*, 968.
- (23) Jho, J. Y.; Yee, A. F. *Macromolecules* **1991**, *24*, 1905.
- (24) Hutnik, M.; Argon, A. S.; Suter, U. *Macromolecules* **1991**, *24*, 5970.
- (25) Eisenberg, A. In *Physical Properties of Polymers*; Mark, J. E., Eisenberg, A., Graessley, W. W., Mandelkern, L., Koenig, J. L. Eds.; American Chemical Society: Washington, DC, 1984; p 93.
- (26) Taylor, M. G.; Sundararajan, P. R. *Macromolecules* **1990**, *23*, 2602.
- (27) Petrie, S. E. B.; Moore, R. S.; Flick, J. R. *J. Appl. Phys.* **1972**, *43*, 4318.
- (28) Kambour, R. P.; Carbeck, J. D.; Nachlis, W. L. *J. Non-Cryst. Solids* **1991**, *131-133*, 563.

**Registry No.** PY-DPH, 142320-40-9; CZ-DPH, 142320-41-0; EA-DPH, 125948-64-3; A-PCR (copolymer), 25037-45-0; A-PCR (SRU), 24936-68-3; C-PCR (copolymer), 26570-63-8; C-PCR (SRU), 26500-24-3; Z-PCR (copolymer), 26471-16-9; Z-PCR (SRU), 25135-52-8.